A miniature, 500 000 rpm, electrically driven turbocompressor

Daniel Krähenbühl
Student Member IEEE
Power Electronic System Laboratory
ETH Zurich
CH-8092 Zurich, Switzerland
kraehenbuehl@lem.ee.ethz.ch

Christof Zwyssig
Student Member IEEE
Celeroton Ltd.
Gloriastrasse 35
CH-8092 Zurich, Switzerland
christof.zwyssig@celeroton.com

Hansjörg Weser
High Speed Turbomaschinen GmbH
Nikolaus-Otto-Straße 17
D-38165 Lehre (Wolfsburg), Germany
h.weser@hsturbo.de

Johann W. Kolar
Senior Member, IEEE
Power Electronic System Laboratory
ETH Zurich
CH-8092 Zurich, Switzerland
kolar@lem.ee.ethz.ch

***Abstract* -- The trend in compressors for fuel cells, heat pumps, aerospace and automotive heating, ventilation and air conditioning systems, is towards ultra-compact size and high efficiency. This can be achieved by using turbocompressors instead of scroll, lobe or screw compressors, increasing the rotational speed and employing new electrical drive system technology and materials. This paper presents a miniature, electrically driven two stage turbocompressor system running at a rated speed of 500 000 rpm. The design includes the thermodynamic analysis, the electric motor, the inverter, the control and the system integration with rotor dynamics and thermal considerations. Experimental measurements such as the compressor map are presented for air under laboratory conditions. The two stage turbocompressor has been tested up to a speed of 600 000 rpm, where a maximal pressure ratio of 2.3 at a mass flow of 0.5 g/s has been reached. To the authors knowledge this is the highest rotational speed achieved with an electrically driven turbocompressor.**

***Index Terms* -- Electric drives, permanent-magnet (PM) machines, turbocompressor, ultrahigh-speed.**

I. Introduction

In future cars and airplanes more and more hydraulic, pneumatic and mechanical systems, also compressors will be replaced with electrically driven systems: the trend is to more-electric aircrafts and vehicles. Examples are the compressors for heating, ventilation and air conditioning (HVAC) in cars or air pressurization for aircraft cabins. The power levels of these electrically driven compressors are from about 100 watts up to a few kilowatts. Additionally, several car manufacturers have research projects or even prototypes on electric vehicles with fuel cell propulsion systems, or a fuel cell system as range extender. Also in trucks and aircrafts, fuel cells are planned to be used as auxiliary power units. A manned aircraft with a fuel cell/lithium-ion battery hybrid system to power an electric motor coupled to a conventional propeller, successfully completed a flight in Spain [1]. At Georgia Institute of Technology, unmanned fuel cell-powered aerial vehicles (UAVs) have been designed and tested [2]. All these fuel cells usually need an electrically driven air compressor which consumes around 10-20% of the output power of the fuel cell, and the pressure levels are usually between 150 and 250 kPa [3]. The electrically driven air compressor should be small, lightweight and efficient.

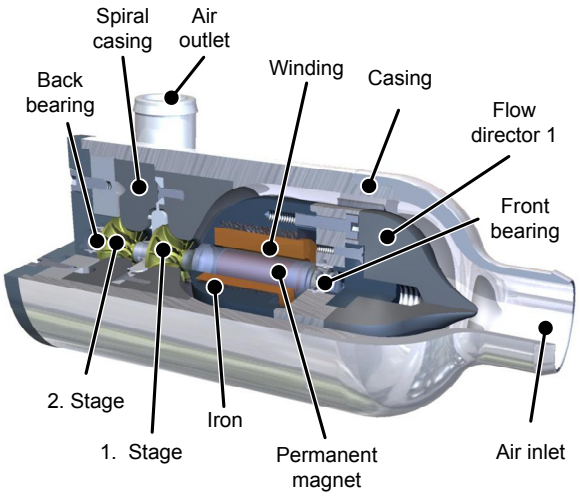

Fig. 1 Cross section view of the integrated two stage electrically driven turbocompressor system.

Other applications for electrically driven compressors are residential applications like heat pumps, in order to enable a more rational use of energy [4]. Also there, the trend is to more compact systems with a higher efficiency. Distributed heat pump systems could be realized with smaller compressors and expanders.

All of these applications need ultra-compact, high-efficient, electrically driven compressor systems and they have a strong link to renewable energy systems. Turbocompressors have both in size and efficiency advantages over other compressor types, such as scroll, lobe or screw compressors [3]. In both turbomachinery and electrical machines, power density increases with increasing

rotational speed [5], [6]. Therefore, these systems ideally have rotational speeds between 100 000 rpm and 1 Mrpm at power levels of a few 100 watts up to several kilowatts.

In this paper, a miniature two stage electrically driven turbocompressor system is presented. It has a rated rotational speed of 500 000 rpm for a calculated air pressure ratio of 2.25 and a mass flow of 1 g/s at ambient conditions for temperature and inlet pressure. The system is designed for the cabin air pressurization system of the Solar Impulse airplane [7], but the specifications are in the area of the other applications mentioned. The design is based on a one stage electrically driven compressor built as a first prototype [8]. The two stage version of the compressor is required for an increase in pressure ratio. This is necessary because the maximum flying altitude will be around 12 000 m. The system is shown in Fig. 1 and Fig. 5, it comprises of two radial impellers, a permanent-magnet (PM) motor and the power and control electronics. The paper starts with the main scaling laws of turbomachinery, electrical machine and power and control electronics and then describes the different components electrical machine, power electronics and turbomachinery, as well as the system integration including thermal and rotordynamic design. Finally, measurement results are presented.

II. Scaling Laws

There are two reasons for downscaling turbomachinery. Firstly, in high power applications the power density can be increased with modularization and secondly, new emerging applications demand compressors with lower mass flow at constant pressure ratios. In [5] is shown that the power density (*P/V*) of turbomachinery is inversely proportional to the rotor diameter *D* of the turbomachinery:

$$\frac{P}{V} \propto \frac{1}{D} . \qquad (1)$$

This implies that a conventional turbomachine with a certain output power can get replaced with a number of smaller units which have all together the same total output power but a smaller overall volume. This scaling implies constant surface speed, which means, that the rotational speed scales inversely proportional with the diameter *D*, shown in (4). However, this is not fully accurate, as a mayor condition for scaling of turbomachinery is a constant Reynolds number, which is also proportional to the dimension of the flow channel and the height of the air flow channel d_h, shown in (2). Since the Reynolds number decreases with miniaturization and does not remain constant, the power density increases less than *1/D*.

$$\mathrm{Re} = \frac{c d_h}{\nu} . \qquad (2)$$

As an example, one large turbocompressor can be replaced with 16 compressors, each with a volume of 1/64 of the conventional compressor, which together has the same output power but requires only a quarter of the volume of the conventional compressor. The diameter of the small units would be ¼ of the original one and the rotational speed would therefore increase by a factor of at least 4.

The requirements for turbocompressors, like the Solar Impulse cabin air pressurization system, but also the other mentioned applications such as heat pumps and fuel cell compressors, demand low flow rates (e.g. 1 g/s to 20 g/s) at relatively high pressure ratios (e.g. 1.3 to 3). The characteristic parameters volume flow $\dot{V}$, specific pressure head *Y* and rotational speed *n* can be compiled in the non-dimensional parameter specific speed σ

$$\sigma = \frac{2 \cdot \phi^{1/2}}{\psi^{3/4}} = \frac{n \cdot \sqrt{\dot{V}}}{(2 \cdot Y)^{3/4}} \cdot 2 \cdot \sqrt{\pi} . \qquad (3)$$

This parameter is composed of the flow coefficient ϕ and pressure coefficient ψ. Downscaling of a macro turbomachine for constant specific speed and lower volume flow therefore leads to an increase in rotational speed.

The power density in electrical machines scales with speed (4),

$$\frac{P}{V} \propto n . \qquad (4)$$

Therefore, the overall volume of the electrical machines in the example above is also ¼ of the original one.

In contrast to electrical machines, the size of the power electronics mainly scales with the power rating and is minimized by choosing the correct topology, through efficiency improvements and the use of high switching frequencies in order to reduce the volume of passive components. For systems with high power ratings, the size of the control electronics is negligible compared to the power electronics. However, for ultrahigh-speed machines with low power ratings (e.g. 100 W), the control electronics size becomes significant. Generally, the size of the control electronics scales with the complexity of the control method selected and the complexity depends on the topology and the modulation schemes used.

III. Electrical Machine

The challenges in the machine design are the mechanical rotor design, especially the stresses in the permanent magnet, and the minimization of high-frequency losses due to eddy-currents in copper and iron and air friction.

The PM machine has been optimized for lowest losses, regarding several constraints e.g. maximal active length,

maximal iron diameter, minimal sleeve thickness, minimal air gap, etc. For this reason, an optimization method has been developed which takes air friction losses, iron losses, copper losses, and eddy current losses into account [10]. The machine has been optimized for rated power of 150 W, which results from the thermodynamic design for an inlet temperature of 220 K and a pressure ratio of 2.25 at an inlet pressure of 444 kPa. However, under laboratory conditions the inlet temperature is 300 K and therefore the required power is 350 W, which leads to higher ohmic losses in the windings (34.4 W at laboratory conditions compared to 6.8 W at rated conditions). The thermal design has therefore been done for laboratory conditions, see section VI.

The rotor of the PM motor consists of a diametrically magnetized cylindrical SmCo permanent magnet encased in a retaining titanium sleeve ensuring sufficiently low mechanical stresses on the magnet. The eccentricity is minimized by shrink fitting the sleeve onto the permanent magnet and grinding the rotor.

The PM generator utilizes two high-speed ball bearings due to its simplicity and small size (inner diameter: 3.175 mm, outer diameter: 6.35 mm, l = 2.8 mm). The ball bearings are assembled at each end of the rotor, in order to be able to change them without the need for disassembling the impellers.

The stator magnetic field rotates with high frequency (8.3 kHz), it is therefore necessary to minimize the losses in the stator core by using amorphous iron, and the eddy-current losses in the air-gap winding by using litz-wire. The optimization of the machine dimensions shows that air friction losses influences the optimum design considerably, leading to small rotor diameter and therefore reduced air friction losses, but slightly increased copper losses. Despite the high speed operation, the machine efficiency at rated power is 90% including air friction and ball bearing losses. A detailed description of the machine design has been presented in [9], while the optimization process has been presented in [10]. In Table I calculated machine data and in Table II calculated machine losses are summarized.

Considering the rated torque and the rotor inertia the maximal acceleration (*dn/dt*) is 1 million rpm/s. However, the dynamic performance of the speed controller has been limited to 40 krpm/s, in order to prevent additional friction in the ball bearings.

IV. INVERTER

The bi-directional pulse amplitude modulation (PAM) inverter consists of a standard 3-phase inverter, an additional buck converter and a DSP-based control system. The inverter part is controlled in six-step or block commutation mode, which means that each switch is conducting for 120° electrical degrees, and therefore, switched with the fundamental frequency of the machine. The phase currents are controlled via the buck converter. The dc-current is measured for the torque controller, while the stator voltages are measured for the sensorless rotor position detection and

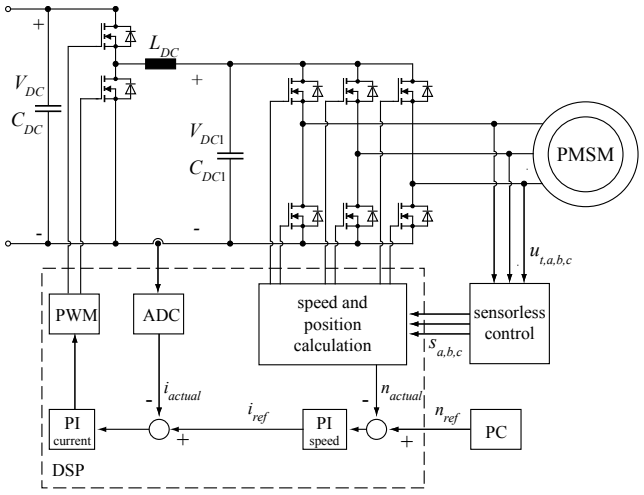

Fig. 2 Pulse amplitude modulation (PAM) power electronics and control system for driving an ultrahigh-speed permanent-magnet machine.

TABLE I
ELECTRICAL MACHINE DATA

Description	Value	Unit
rated speed	500 000	rpm
rated electric power		
inlet temperature 220 K	150	W
inlet temperature 300 K	350	W
rated torque	2.86	mNm
rated machine temperature	120	°C
magnet flux linkage	0.265	mVs
back EMF at rated speed	13.9	V
stator inductance	3.3	µH
stator resistance	0.12	Ω

TABLE II
CALCULATED ELECTRICAL MACHINE LOSSES

Description	Value	Unit
copper losses		
inlet temperature 220 K	6.8	W
inlet temperature 300 K	34.4	W
iron losses	0.65	W
air friction losses	5	W
bearing losses	5	W
total losses (without bearing)		
inlet temperature 220 K	12.5	W
inlet temperature 300 K	40.0	W
machine efficiency (low pressure)		
inlet temperature 220 K	91.7	%
inlet temperature 300 K	88.6	%

for the speed controller. Using a sensorless rotor positioning technique eliminates the disadvantages of rotor position sensors, such as an increased failure probability and an axial extension of the rotor. Especially a longer rotor is unwanted in this application because the critical speeds are lowered. For an inverter with block commutation, the back EMF can directly be measured during the 60° electrical degrees off intervals in each phase.

TABLE III
POWER ELECTRONICS

Description	Value	Unit
rated power	150	W
power electronics efficiency	90	%
dimensions power electronics (b *x* l *x* h)	80 *x* 80 *x* 47	mm
total weight (electronic)	220	g

TABLE IV
TURBOMACHINERY DATA

Description	Value	Unit
rated speed	500 000	rpm
rated pressure ratio	2.25	-
rated mass flow	1	g/s
rotor inertia	$26 \cdot 10^{-9}$	kgm^2
compressor efficiency	74	%
turbocompressor length	80	mm
turbocompressor diameter	35	mm
total weight	140	g

The power electronics has an efficiency of 90 % at rated power. In Table III a summary of important data are shown, while the block diagram of the inverter and the control system is depicted in Fig. 2.

V. TURBOMACHINERY

A radial compressor was chosen, because this type of compressors can generate high pressure ratios at low mass flows with a single stage. However, to achieve the design goal for the pressure ratio of 2.25 at a very low mass flow of 1 g/s, a two stage design is employed. The biggest challenge is the manufacturing of the impeller and the fitting between the different pieces, especially impeller and casing. This is because the manufacturing tolerances cannot be decreased proportional with the downscaling and therefore the leakage losses become more dominant for small compressors. This means that the chosen tip clearance (100 µm) is rather high. For a further investigation of the influence of the tip clearance, the clearance of the first stage can be adjusted between 0 µm and 100 µm.

The first impeller consists of 12 blades (no splitter blades) and has a mean streamline diameter at the inlet of 5.28 mm, while the outlet diameter is 10.5 mm. The second impeller consists of 12 blades and additional splitter blades and has a slightly smaller mean streamline, while the outlet diameter remains the same. After the flow leaves the second stage, it enters the vane less diffuser and then gets collected in a volute and thereby guided into the exit flange.

The two compressor stages are directly mounted with a shrink fit onto the motor rotor shaft as shown in Fig. 5. Between the two stages, a spacer sleeve is mounted, and the back bearing seat is shrink fitted onto the rotor.

According to the results from the one stage turbocompressor [8], the design pressure ratio is 2.25 at a mass flow of 1 g/s, which is calculated to be achieved at a rotational speed of 500 000 rpm. The power consumption is depending on the mass flow and the inlet temperature of the air, at the design operating point it is 350 W at laboratory conditions. The compressor data is compiled in Table IV.

VI. SYSTEM INTEGRATION

Beside the design of the individual components, an analysis of the mechanical stresses and rotor dynamics of the common rotor of electrical machine and turbomachine, and a thermal design of the entire system are needed. The bending modes of the rotor are depicted in Fig. 3. The length of the shaft is adjusted such that the rated speed falls between the second and the third bending modes. In order to reduce losses and to have enough space for the flow director after the first stage the spacing between the two stages should be as big as possible. However, the third bending mode, which limits the maximum speed, is reduced with an increase of the rotor length. Therefore, the space between the two stages is limited. The bending modes calculations have been made during the machine optimization process with an analytical approach in order to define geometric constraints for the machine. The final rotor dynamic design has been verified with 3D FE simulations.

The main cooling of the motor and the bearings is due to the air flow; the input air first circulates around the motor and bearing 1 and thereby cools them. Because of this special design no additional cooling fins are needed to guarantee safe operation under laboratory conditions. The most critical spot is ball bearing 2, which produces high losses and has worse cooling conditions than bearing 1. The maximal allowed temperature in the bearings is 200°C. A thermal FE analysis of the integrated system under laboratory conditions, including the calculated losses, can be found in the cross-section view in Fig. 4. It can be seen that the temperatures in ball bearing 2 do not exceed 110°C.

VII. TEST BENCH SETUP

An experimental test bench is built in order to verify theoretical considerations and the feasibility of such ultra-compact ultrahigh-speed electrically driven turbocompressor systems. Therefore, two valves are connected to the compressor inlet and outlet respectively for setting the input and output pressure conditions. When the first valve is fully open, the second valve acts as a variable load, and therefore measurements in over pressure condition can be performed. For low pressure conditions the second valve is open and the input pressure is adjusted using the first valve. A pressure sensor and a thermocouple are placed between the compressor output and the valve. At the compressor inlet a pressure sensor, a thermocouple and a mass flow sensor are used. Additionally, two thermocouples are used to monitor the power electronic and motor winding temperature. Due to the fact that the motor is of synchronous type, the speed does

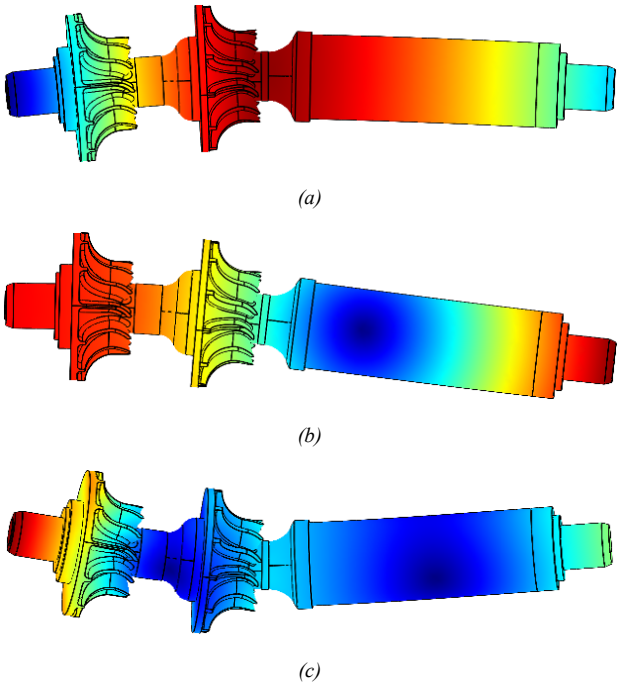

Fig. 3 Bending modes of the two stage miniature turbocompressor rotor. First bending mode at 2.6 kHz, 156 krpm (a), second bending mode at 5.9 kHz, 354 krpm (b), and third bending mode at 12 kHz, 720 krpm (c). The color shows the displacement: no displacement (blue), maximal displacement (red).

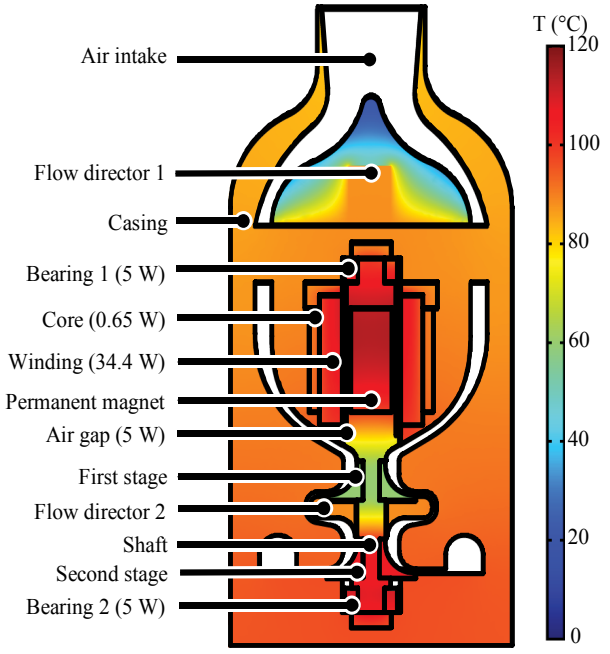

Fig. 4 FE simulations of the temperature distribution under laboratory conditions, at 500 000 rpm and a drive power of 350 W, assuming an inlet temperature of 300 K.

not have to be measured separately. All measured data is collected by the DSP-based control system and is transmitted to a PC for online and offline analysis.

VIII. MEASUREMENTS

First, the compressor map depicting the pressure ratio versus mass flow for different rotational speeds is measured. Two different tip clearances are tested (35 µm and 70 µm) and both over and low pressure conditions are verified. In Fig. 7 it can be seen that at the rated speed of 500 000 rpm a pressure ratio of 1.95 is achieved with a tip clearance of 35 µm, while the maximum pressure ration drops to 1.9 with a tip clearance of 70 µm (Fig. 9). This is lower than the prediction of 2.25. One main factor for this difference is the mechanical tolerances in the manufacturing which are not sufficiently small yet, which results in leakage and secondary air flow. Also, the two stage design needs a flow director with small radii between the two stages, which leads to additional pressure drop, compared to the one stage turbocompressor system [8]. In Fig. 10 the electric power consumption of the turbocompressor system is shown.

In Fig. 8 the maximal pressure ratios of the one and two stage compressors are compiled. It can be seen that the predicted pressure ratio of the two stage compressor of 2.25 is reached at a speed of 600 000 rpm, while the one stage compressor would reach this ratio at 800 000 rpm, which is clearly too high for ball bearings.

The compressor efficiency can be calculated from the measured pressure ratio and the input and output air temperatures with.

$$\eta_i = \frac{T_1\left[\left(\frac{p_2}{p_1}\right)^{\frac{\kappa-1}{\kappa}} - 1\right]}{T_2 - T_1} \quad (5)$$

The input air temperature measurement is located directly before the first compressor stage in order not to include the air heating by the motor. Due to the compact design it is not possible to measure the temperature between the first and second stage, therefore, no individual stage efficiencies can be measured.

Due to the same reasons as the measured pressure ratio is lower than the estimated, the measured efficiency (60%) is lower than calculated (74%).

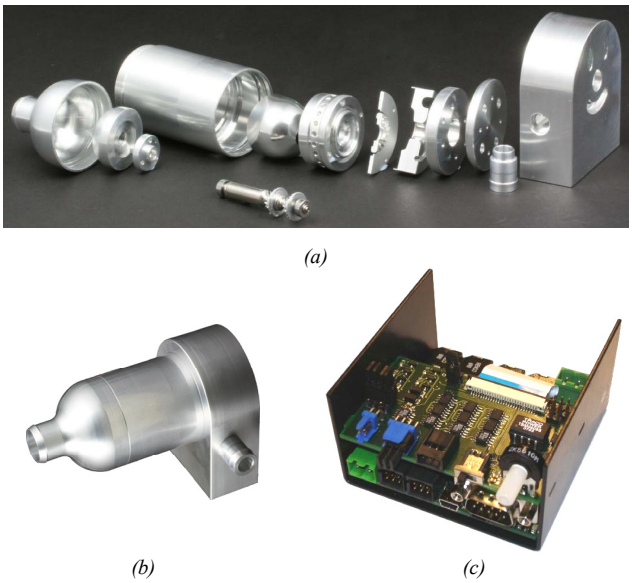

Fig. 5. Miscellaneous components of the miniature two-stage electrically driven compressor (a), the assembled miniature two-stage electrically driven compressor (80 x 35 mm) (b) and the power and control electronics including measurements of massflow, pressure and temperature (80 x 80 x 47 mm) (c).

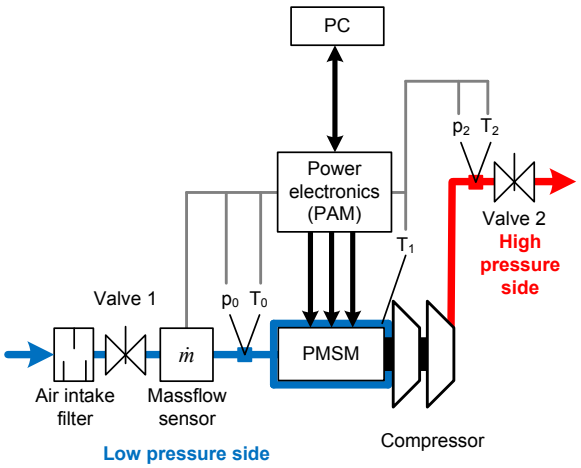

Fig. 6 Test bench setup including massflow sensor, two valves (for over and low pressure) and two thermocouples for temperature monitoring.

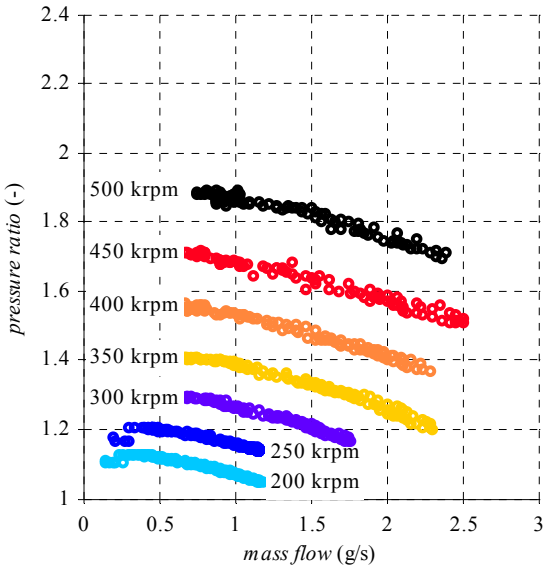

Fig. 7 Measured over pressure compressor map of the miniature turbocompressor, with a clearance of 35 µm at the first compressor wheel.

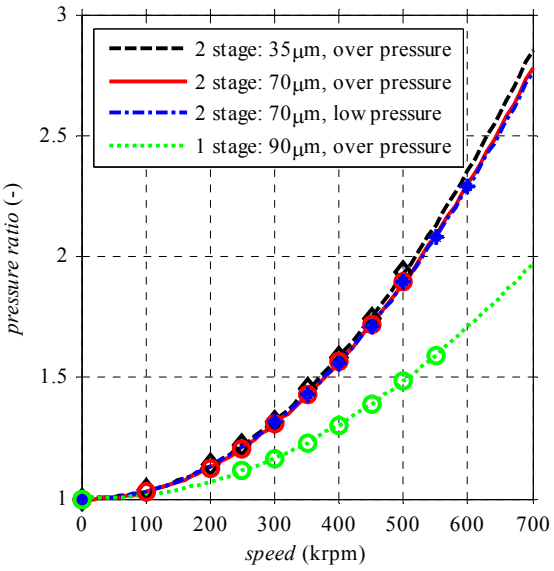

Fig. 8 Measurements and interpolation of maximal pressure ratio for over and low pressure conditions and for 70 µm and 35 µm clearance. The green dashed line indicates the maximal pressure ratio for the one stage compressor for a clearance of approximately 90 µm.

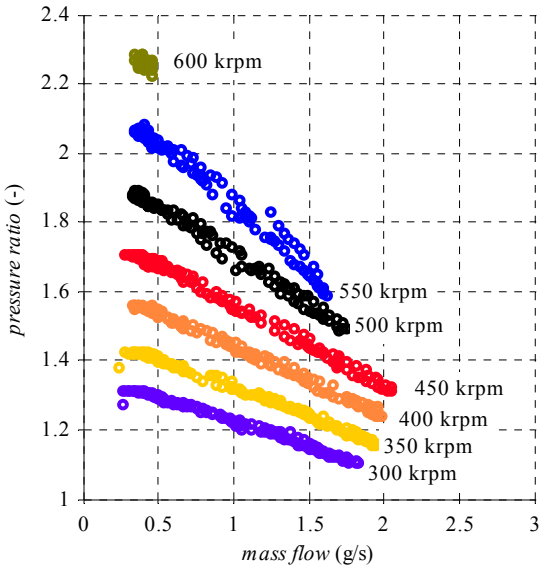

Fig. 9 Measured low pressure compressor map of the miniature turbocompressor, with a clearance of 70 µm at the first compressor wheel.

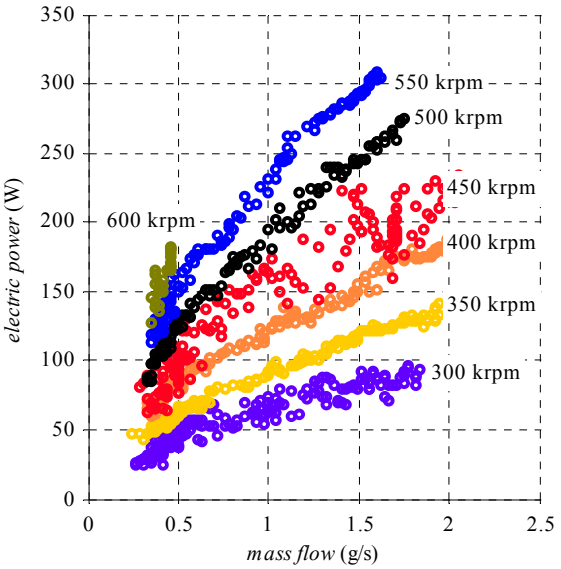

Fig. 10 Measured electric power consumed by the high speed electric drive system of the miniature turbocompressor at low pressure conditions.

IX. Conclusion

This paper presents the design of a miniature, 500 000 rpm electrically driven turbocompressor for various applications in the area of air and gas pressurization for future automotive, aerospace and residential applications with a strong link to renewable energy systems. The system design is based on an electrical drive system achieving highest rotational speeds. The manufacturing of miniaturized compressors represents difficulties due to smallest contours and desirably small tolerances. However, measurements show that despite this difficulties the system has a performance close to the specified design operating point, and turbocompressors with speeds even above 500 000 rpm are feasible.

This new system fulfils the specification regarding the mass flow and the rotational speed, but it does not yet achieve the necessary pressure ratio. One next step in the project will be to decrease the clearances between the compressor stages and the casing as well as between the second flow director and rotor further. In a second step a redesign of the compressor wheels will be undertaken.

Bearing lifetime is the main challenge before such ultrahigh-speed electrically driven compressors can get widely used in industry. For reaching acceptable lifetime and oil-free compressor systems the high speed ball bearings must be replaced by air bearings or magnetic bearings.

References

[1] Lapeña-Rey N., Mosquera J., Bataller E., Ortí F., The Boeing Fuel Cell Demonstrator Airplane, *AeroTech Congress & Exhibition*, September 2007, Los Angeles, CA, USA.

[2] Bradley H.T., Moffitt A.B., Thomas W. R., Mavris D., Parekh E.D., Test Results for a Fuel Cell-Powered Demonstration Aircraft, *Power Systems Conference*, November 2006, New Orleans, LA, USA.

[3] Blunier B., Miraoui A., Air Management in PEM Fuel Cell: State-of-the-Art and Prospectives *International Aegean Conference on Electrical Machines and Power Electronics*, Electromotion 2007, Bodrum, Turkey, Sept. 10-12, 2007.

[4] J. Schiffmann, "Integrated Design, Optimization and Experimental Investigation of a Direct Driven Turbocompressor for Domestic Heat Pumps," Ph.D. dissertation, Ecole Polytechnique Federale de Lausanne, Switzerland, 2008.

[5] Kang S.,. Lee S.-J.J, Prinz F.B.. Size does matter, the pros and cons of miniaturization. ABB Rev. 2 (2001) 54–62.

[6] Binder A., Schneider T., "High-Speed Inverter-Fed AC Drives," *International Aegean Conference on Electrical Machines and Power Electronics*, Electromotion 2007, Bodrum, Turkey, Sept. 10-12, 2007.

[7] www.solarimpulse.com

[8] Zwyssig, C., Krähenbühl, D., Weser, H., Kolar, J.W., A Miniature Turbocompressor System, *Proceedings of the Smart Energy Strategies 2008 (SES 2008)*, Zurich, Switzerland, Sept. 8 - 10, 2008 .

[9] Zwyssig C., Kolar J.W., Design Considerations and Experimental Results of a 100 W, 500 000 rpm Electrical Generator, *Journal of Micromechanics and Microengineering*, Issue 9, pp. 297 - 302, Sept. 2006.

[10] Luomi, J., Zwyssig, C.; Looser, A.; Kolar, J.W., Efficiency Optimization of a 100-W, 500 000-rpm Permanent-Magnet Machine Including Air Friction Losses, *Industry Applications Conference, 2007. 42nd IAS Annual Meeting. Conference Record of the 2007 IEEE*, vol., no., pp.861-868, 23-27 Sept. 2007